Eur. Phys. J. D **46**, 195–202 (2008)
DOI: 10.1140/epjd/e2007-00288-0

THE EUROPEAN PHYSICAL JOURNAL D

Nanoplasma dynamics in Xe clusters driven by ultraintense laser fields

A. Heidenreich, I. Last, and J. Jortner[a]

School of Chemistry, Tel-Aviv University, 69978 Tel-Aviv, Israel

Received 5 July 2007 / Received in final form 3 September 2007
Published online 12 October 2007 –

Abstract. We present a theoretical and computational study of the properties and the response of the nanoplasma and of outer ionization in Xe_n clusters ($n = 55$–2171, initial cluster radius $R_0 = 8.7$–31.0 Å) driven by ultraintense near-infrared laser fields (peak intensity $I_M = 10^{15}$–10^{20} Wcm^{-2}, temporal pulse length $\tau = 10$–100 fs, and frequency $\nu = 0.35$ fs^{-1}). The positively charged high-energy nanoplasma produced by inner ionization nearly follows the oscillations of the fs laser pulse and can either be persistent (at lower intensities of $I_M = 10^{15}$–10^{16} Wcm^{-2} and/or for larger cluster sizes, where the electron energy distribution is nearly thermal) or transient (at higher intensities of $I_M = 10^{18}$–10^{20} Wcm^{-2} and/or for smaller cluster sizes). The nanoplasma is depleted by outer ionization that was semiquantitatively described by the cluster barrier suppression electrostatic model, which accounts for the cluster size, laser intensity and pulse length dependence of the outer ionization yield. The electrostatic model was further utilized for estimates of the laser intensity and pulse width dependence of the border radius $R_0^{(I)}$ for the attainment of complete outer ionization at $R_0 \lesssim R_0^{(I)}$, while at $R_0 > R_0^{(I)}$ a persistent nanoplasma prevails. $R_0^{(I)}$ establishes an interrelationship between electron dynamics and nuclear Coulomb explosion dynamics in ultraintense laser-cluster interactions.

PACS. 36.40.Gk Plasma and collective effects in clusters – 31.15.Qg Molecular dynamics and other numerical methods – 36.40.Wa Charged clusters

1 Introduction

Remarkable advances in the realm of ultrafast processes pertain to electron dynamics, involving changes in the electronic states of atoms and molecules, with the nuclear motion being frozen [1–6]. The experimental interrogation of ultrafast processes with the temporal resolution of electron motion was accomplished for inner-shell electron dynamics [4], real-time interrogation of attosecond electron tunneling [5], and the application of a single (or sub-) near-infrared laser cycle [6] for nonsequential double ionization $(e, 2e)$ electron recollision processes [3] in atoms and diatomic molecules. Other novel facets of electron dynamics are exhibited in elemental and molecular clusters driven by ultraintense, femtosecond laser fields [7–11] (peak intensities [12] $I_M = 10^{15}$–10^{21} Wcm^{-2}). The many-electron system is produced by a compound, extreme cluster ionization process [7–11]. It involves three sequential-parallel processes: (i) inner cluster ionization, (ii) the formation of a nanoplasma consisting of cluster positive ions and an 'electron cloud' within the cluster or its vicinity, and (iii) outer cluster ionization [8–11]. The nanoplasma, which is produced by strong-field ionization, responds to the laser field on the time scale of half of the laser cycle [10,13] (i.e., ∼1.5 fs for a near-infrared laser). Macroscopic models for the nanoplasma rested on a 'plasma model' [7,8, 14], with collective electron excitations being attained by resonance heating (via one-photon laser absorption) of a macroscopic spherical plasma with a 'critical' density (attained in the course of cluster Coulomb explosion (CE)). More elaborate descriptions of nonlinear resonant absorption of a near-infrared laser in the nanoplasma, which involves inverse bremsstrahlung collisions [15] and energetic electrons transiting through the cluster [16], were recently provided. Molecular dynamics (MD) simulations [7–11,13, 14,17–28] are useful for the assessment of the applicability and validity of such macroscopic models.

The properties and response of the nanoplasma result in cluster outer ionization, which constitutes the subject matter of this paper. We report on MD simulations of high-energy electrons and ions for Xe_n clusters driven by an ultraintense near-infrared laser field. From the present study new information emerges on the outer ionization levels, on the nanoplasma properties (population, density and electron energetics) and on the nanoplasma dynamics. The cluster outer ionization, which involves the (partial or complete) sweeping out of the nanoplasma electrons in the laser field, was modeled by the entire cluster barrier suppression ionization (CBSI) model, which was introduced by Last and Jortner [10,19,20], and subsequently considered by Saalmann and Rost [21]. In this paper we

[a] e-mail: jortner@chemsg1.tau.ac.il

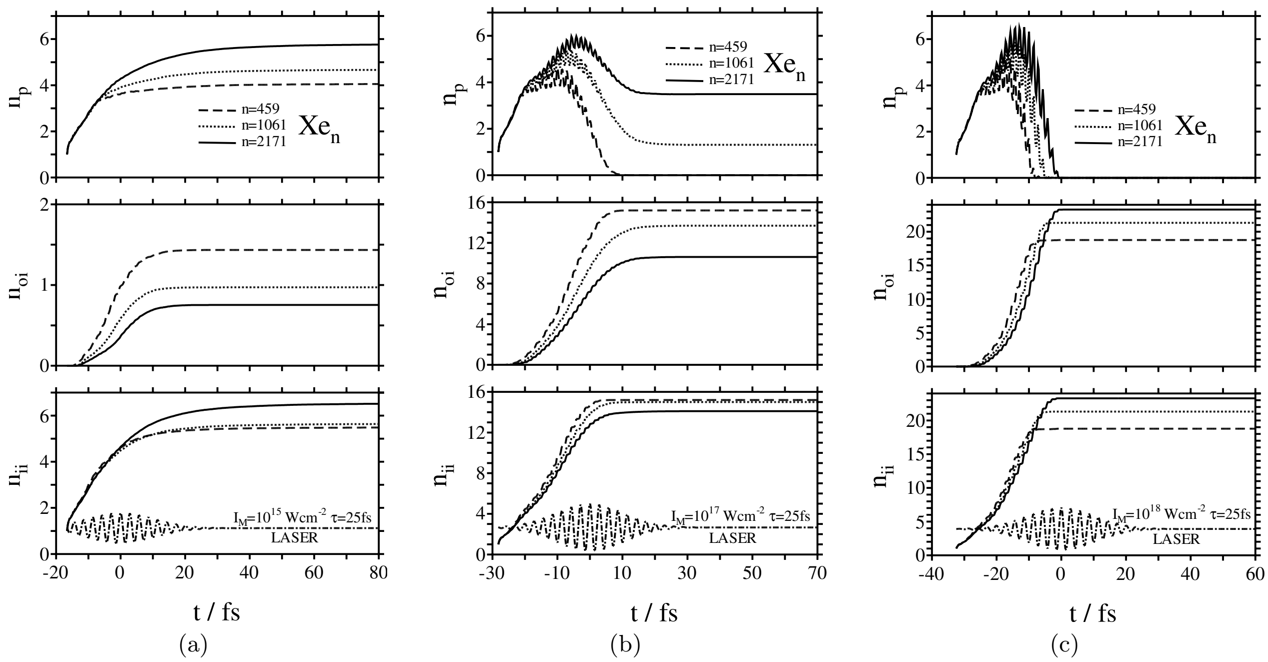

Fig. 1. The time dependence of the inner ionization levels n_{ii}, the outer ionization levels n_{oi} and the nanoplasma population $n_p = n_{ii} - n_{oi}$ for Xe_n clusters (n = 459, 1061 and 2171 as marked on the panels) for the intensities $I_M = 10^{15}$ Wcm^{-2} (a), $I_M = 10^{17}$ Wcm^{-2} (b), and $I_M = 10^{18}$ Wcm^{-2} (c). The laser pulse width is $\tau = 25$ fs. The electric fields of the Gaussian laser pulses ($- \cdot - \cdot -$), expressed in arbitrary units for $t \geqslant t_s$, are marked LASER.

confront the simulation results for nanoplasma electron dynamics with the CBSI model, establishing the pulse intensity and cluster size dependence of the outer ionization levels. Subsequently we characterized the nanoplasma response in Xe_n clusters in terms of the cluster border radius $R_0^{(I)}$ for complete outer ionization [19,20,22]. In previous work [19,22] on $(D_2)_{n/2}$ clusters, the laser intensity and pulse length dependence of $R_0^{(I)}$ were theoretically studied for a nanoplasma produced by complete cluster inner ionization, with the energetics of CE under conditions of partial outer ionization being determined by $R_0^{(I)}$ [22]. Recent applications of this concept for the analysis of experimental data for CE of $(H_2)_{n/2}$ clusters were presented [23]. In the present work we report on the features of $R_0^{(I)}$ in a many-electron elemental Xe_n cluster, where the inner ionization level exhibits strong intensity dependence. This analysis establishes the cluster size, laser intensity and pulse length dependence of $R_0^{(I)}$ for Xe_n clusters, a parameter of considerable importance for the optimization of the high energy of the ions in the CE of these multicharged clusters.

2 Properties of the nanoplasma

MD simulations of (high-energy) electrons and ions were conducted for Xe_n (n = 55–2171) clusters driven by an ultraintense, Gaussian, infrared laser field. The laser pulse was characterized by a temporal onset at $t = t_s$ ($t_s < 0$) [11], a peak at $t = 0$, near termination at $t = -t_s$, peak intensities $I_M = 10^{15}$–10^{20} Wcm^{-2}, pulse temporal widths τ = 10–100 fs, pulse frequency $\nu = 0.35$ fs^{-1} and photon energy 1.44 eV. The MD simulation scheme was previously described [10,11]. The criterion for outer ionization was that the distance of an electron from the center of mass of the cluster exceeded six times the radius $R(t)$ of the expanding cluster [10,11] ($R(t)$ is determined by the configuration of the ions). Similar results (within 20%) were obtained for the outer ionization level by increasing this cut-off distance from $6R(t)$ to $10R(t)$. Our characterization of outer ionization considers those nanoplasma electrons that are swept away from the cluster by the laser field. Our criterion specifies that the outer ionized electrons be located outside a cut-off radius of (6–10)$R(t)$. The choice of the large cut-off radius is necessary, as nanoplasma electrons can be driven back inside the vicinity of the $R(t)$ on the time scale of the laser period [10,13]. Our specification of the outer ionization differs from that of Petrov and Davis [18], who distinguished between inner electrons within the cluster radius $R(t)$ and outer electrons outside $R(t)$. Our approach, which introduces a large cut-off radius for outer ionization, accounts for the gross features of laser driven nanoplasma electron detachment from the cluster to form the macroscopic plasma filament within an assembly of clusters [10,11,14].

Figure 1 presents the simulation results for the time dependence of the outer ionization and nanoplasma population in Xe_n clusters (n = 459, 1061 and 2171) at intensities of $I_M = 10^{15}$, 10^{17}, and 10^{18} Wcm^{-2}. The time-dependent inner ionization levels [11], which correspond to the total number N_{ii} of electrons produced by barrier suppression ionization and electron impact ionization within the cluster [10,11] with $n_{ii} = N_{ii}/n$ electrons per constituent, are also presented in Figure 1. The total number of electrons that were depleted by outer ionization is N_{oi} (with $N_{oi} \leqslant N_{ii}$), while the outer ionization level per constituent atom is given by

$$n_{oi} = N_{oi}/n. \quad (1)$$

The total number of electrons in the nanoplasma is $N_p = N_{ii}–N_{oi}$ and the number $n_p = N_p/n$ of the electrons in the nanoplasma per constituent atom is

$$n_p = n_{ii} - n_{oi}. \quad (2)$$

The time dependence of $n_{oi}(t)$ and $n_p(t)$ in the cluster size domain $n = 459-2171$ and laser intensity range $I_M = 10^{15}–10^{18}$ Wcm^{-2}, with $\tau = 25$ fs, reveals the following features.

(1) Saturation of the outer ionization level (Fig. 1). The saturation or near-saturation of the outer ionization level is exhibited at times longer than those for the inner ionization level at the same I_M. The saturation of $n_{oi}(t)$ at longer times at $I_M > 10^{16}$ Wcm^{-2} is qualitatively different from the near-saturation of $n_{oi}(t)$ vs. t at $I_M = 10^{15}$ Wcm^{-2}, as the characteristic time for the attainment of the saturation of $n_{oi}(t)$ becomes shorter with increasing I_M. At $I_M = 10^{18}$ Wcm^{-2}, the saturation of $n_{oi}(t)$ is exhibited at the laser peak ($t = 0$), while for $I_M = 10^{15}$ Wcm^{-2} $n_{oi}(t)$ reaches near-saturation at the termination of the laser pulse ($t = -t_s$). This difference reflects on the existence of a persistent nanoplasma in the lower intensity domain and of a transient nanoplasma in the high intensity domain (point (4)).

(2) Relations between limiting inner and outer ionization levels (Fig. 1). For the three cluster sizes studied herein, $n_{oi}^L < n_{ii}^L$ for $I_M \leqslant 10^{16}$ Wcm^{-2}, while $n_{oi}^L = n_{ii}^L$ for $I_M \geqslant 10^{17}$ Wcm^{-2} where $n_{ii}^L = n_{ii}(t_L)$, and $n_{oi}^L = n_{oi}(t_L)$, with $t_L = 90$ fs marking the long-time, temporal end of the trajectories.

(3) The cluster size dependence of the limiting outer ionization levels (Fig. 1). The n_{oi}^L values exhibit an irregular cluster size dependence for different values of I_M. While at $I_M = 10^{15}$, 10^{16} (not shown) and 10^{17} Wcm^{-2} n_{oi}^L decreases with increasing the cluster size, at $I_M = 10^{18}$ Wcm^{-2} n_{oi}^L increases with increasing n. Decreasing n_{oi}^L values with increasing n, as observed for $I_M = 10^{15}–10^{17}$ Wcm^{-2}, originates from the ability of the ionic cluster framework to retain electrons with respect to outer ionization. The qualitative difference at 10^{18} Wcm^{-2} is due to the increase of n_{ii}^L with increasing n, together with a sufficiently strong laser field, which is able to remove all generated nanoplasma electrons by outer ionization even from the largest considered cluster.

(4) Persistent and transient nanoplasma (Fig. 1). For $I_M = 10^{15}–10^{16}$ Wcm^{-2}, the number of electrons in the nanoplasma $n_p(t)$, equation (2), nearly saturates at long times with $n_p^L = n_p(t_L)$ increasing with increasing n, as expected on the basis of the limiting outer ionization level in this intensity domain (point (2)). On the other hand, at $I_M = 10^{18}$ Wcm^{-2}, the nanoplasma is completely depleted before the laser pulse reaches its peak, with the depletion process being more efficient with decreasing n, as manifested by the appearance of a maximum of $n_p(t)$ with a lower field amplitude at lower values of n. At the intensity of $I_M = 10^{17}$ Wcm^{-2}, $n_p(t)$ exhibits an intermediate type of behavior, revealing long time saturation for larger clusters ($n = 1061$ and 2171), and complete depletion for smaller clusters ($n = 459$). In conclusion, in the lower intensity range of $I_M = 10^{15}–10^{16}$ Wcm^{-2}, 'long-time' retention of the persistent nanoplasma (on the time scale of >100 fs) is exhibited, while in the highest intensity domain of $I_M \geqslant 10^{18}$ Wcm^{-2} a transient nanoplasma (on the time scale of $\sim\tau$ for $n = 459–2171$) is produced.

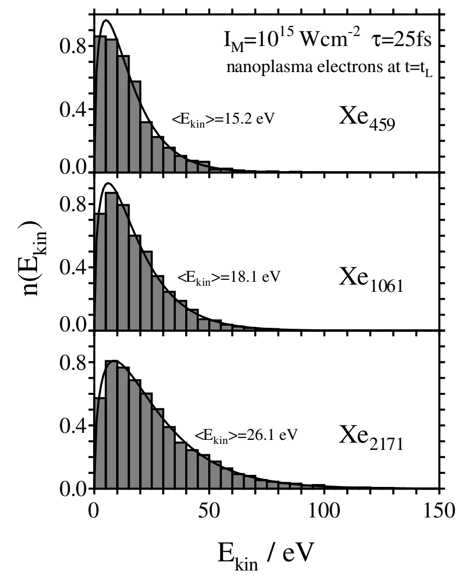

Fig. 2. The kinetic energy distribution of the electrons of a persistent nanoplasma in Xe_{459} clusters ($n_p = 4.1$), in Xe_{1061} clusters ($n_p = 4.9$) and in Xe_{2171} clusters ($n_p = 5.8$). The nanoplasma is produced by interaction with a Gaussian laser pulse ($I_M = 10^{15}$ Wcm^{-2}, $\tau = 25$ fs) and interrogated at a long time $t_L = 92$ fs, where the system is 'laser free' after the termination of the laser pulse.

(5) Energetics of the persistent nanoplasma. In Figure 2 we present the simulation results for the distribution of the kinetic energies of the nanoplasma in Xe_n ($n = 459$, 1061 and 2171) clusters at $I_M = 10^{15}$ cm^{-1} at the 'laser-free' long times of $t = t_L$. The electron kinetic energies E_{kin} of the transient nanoplasma can be well fit (Fig. 2) by the thermal energy distribution

$$P(E_{kin}) \propto (E_{kin}/\langle E_{kin}\rangle)^{1/2} \exp[-3E_{kin}/2\langle E_{kin}\rangle] \quad (3)$$

where $\langle E_{kin}\rangle$ is the average electron kinetic energy. The average electron kinetic energies, which characterize the thermalized nanoplasma, increase with increasing the cluster size (Fig. 2).

(6) High average electron densities in the nanoplasma (Fig. 3). The average electron density is $\rho_e(t) = n_p(t)/(4\pi/3)R(t)^3$, where $R(t)$ is the time-dependent cluster radius in the course of the trajectory. $R(t) = R_0$ at the onset of the laser pulse, $t = t_s$, while $R(t) > R_0$

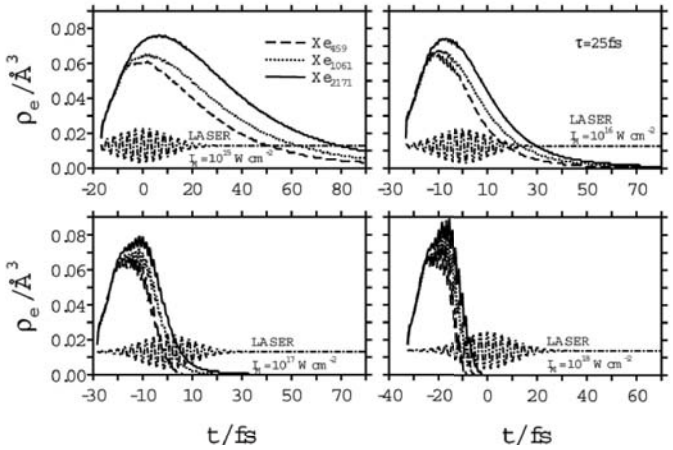

Fig. 3. The time dependent electron density in the nanoplasma $\rho_e(t) = n_p(t)/(4\pi/3)R(t)^3$ in Xe_n clusters ($n = 459$, 1061 and 2171, as marked on the curves). R is the cluster radius obtained from MD simulations. Data are presented for $I_M = 10^{15}$, 10^{16}, 10^{17}, and 10^{18} Wcm^{-2}, as marked on the panels. The Gaussian laser electric fields $(- \cdot - \cdot -)$, expressed in arbitrary units for $t \geqslant t_s$, are presented on the panels.

at longer times due to CE. For the entire I_M range, $\rho_e(t)$ first increases with increasing t, reaching a maximum of $\rho_e^{max} = 0.08$–0.09 Å^{-3}. At $I_M = 10^{18}$ $\mathrm{Wcm}^{-2} \rho_e(t)$ vanishes for $t \geqslant 0$, exhibiting the transient nanoplasma. At $I_M = 10^{17} \rho_e(t)$ decreases towards zero at $t \geqslant 0$, due to a combination of cluster expansion and nanoplasma depletion. For the lowest intensity of $I_M = 10^{15}$ Wcm^{-2}, $\rho_e(t)$ decreases gradually with increasing t on the time scale of 10–90 fs, due to dilution by CE, while retaining a long-time ($t_L = 90$ fs) electron density of $\rho_e = 0.02$ Å^{-3} for Xe_{2171}. The nanoplasma electron densities at the maximum, i.e., $\rho_e^{max} = 8$–9×10^{22} cm^{-3} for the entire I_M domain, and the long-time electron density of $\rho_e = 2 \times 10^{22}$ cm^{-3} at $I_M = 10^{15}$ Wcm^{-2}, are comparable to electron densities in metals.

(7) Subfemtosecond oscillations of the inner/outer ionization levels and of the nanoplasma population. In the intensity range of $I_M = 10^{17}$–10^{18} Wcm^{-2} we observe (Fig. 1) that $n_{ii}(t)$ and $n_p(t)$ exhibit an oscillatory time dependence during the temporal rise of the inner/outer ionization levels. The transient nanoplasma also exhibits such an oscillatory time dependence of $n_p(t)$. A similar response of the nanoplasma was previously reported [13,21]. The period of these temporal oscillations driven by the near-infrared laser is close to half of the laser period ($(2\nu)^{-1} \simeq 1.5$ fs), manifesting the attosecond-femtosecond driving of inner/outer ionization by the ultraintense laser field.

3 Outer ionization

Cluster outer ionization removes all, or part of, the nanoplasma electrons by the laser field [7–10]. Outer ionization was described in terms of a cluster barrier suppression ionization (CBSI) model [10], which is based on the balancing between the cluster exterior Coulomb potential and the laser field potential at the cluster boundary. The CBSI model provides a condition for the occurrence of outer ionization of a cluster of ionic charge $Q_I(t)$ with $N_p(t)$ nanoplasma electrons at the laser field $F_{\ell 0}(t)$ at time t, which is given by [10]

$$F_{\ell 0}(t) = \sqrt{2}\bar{B}\left(Q_I(t) - N_p(t)\right)\Big/[R(t)]^2 \qquad (4)$$

where $F_{\ell 0}(t)$ is the laser field envelope and $\bar{B} = 14.4$ eV. $R(t)$ is the time dependent cluster radius

$$R(t) = \xi(t)R_0 \qquad (4a)$$

where $\xi(t)$ (>1) is the cluster expansion parameter, which originates from CE [10,14,19,20,23]. We consider the long-time values of the Q_I and N_p charges and take the maximal value of the laser field (at $t = 0$), setting $F_{\ell 0}(t) = F_M$, where F_M is related to the laser peak intensity, I_M, by

$$F_M = 2.7448 \times 10^{-7} I_M^{1/2} \qquad (5)$$

where F_M is given in eV Å^{-1} and I_M is given in Wcm^{-2}. The value of $\xi(t)$, equation (4a), is chosen at the peak of the laser pulse ($t = 0$), i.e., $\xi(t) = \xi(0) \equiv \xi$. Taking $Q_I = nn_{ii}^L$, $N_p = nn_p^L$ and $n_{oi}^L = n_{ii}^L - n_p^L$, equation (4) assumes the form

$$F_M = \sqrt{2}\bar{B}n_{oi}^L n/R_0^2\xi^2. \qquad (6)$$

Equation (6), with the simple packing relation $n = 4\pi\rho_A R_0^3/3$ (where ρ_A is the initial atomic density of the neutral cluster), results in the CBSI expression for the outer ionization level, $n_{oi}^L \propto F_M\xi^2/\rho_A R_0$. This result contains several simplifying assumptions inherent in the electrostatic model, in the complete outer ionization at the laser peak ($t = 0$), and in the neglect of an additional contribution of EII at $t > 0$. We shall subsume all these uncertainties into a correction factor γ, with subsequent analyses providing a-posteriori justification for the near-independence of γ on R_0 and on the laser parameters. Equation (6) will be recast in the form

$$n_{oi}^L = F_M\gamma\xi^2 \Bigg/ \left(\frac{4\pi\sqrt{2}}{3}\right)\bar{B}\rho_A R_0. \qquad (7)$$

This result is applicable for the intensity range and cluster size domain where a persistent nanoplasma prevails, i.e., $n_p^L = n_{ii}^L - n_{oi}^L > 0$ (or $n_{ii}^L > n_{oi}^L$). The use of equation (7) gives

$$n_{oi}^L = AI_M^{1/2}/R_0 \qquad (8)$$

where

$$A = 2.745 \times 10^{-7}\gamma\xi^2/(4\pi\sqrt{2}/3)\bar{B}\rho_A. \qquad (9)$$

In equations (8) and (9) I_M is given in Wcm^{-2}, R_0 in Å, and ρ_A in Å^{-3}. For Xe_n clusters with $\rho_A = 0.017$ Å^{-3}, equation (9) results in

$$A = 1.89 \times 10^{-7}\gamma\xi^2 \qquad (10)$$

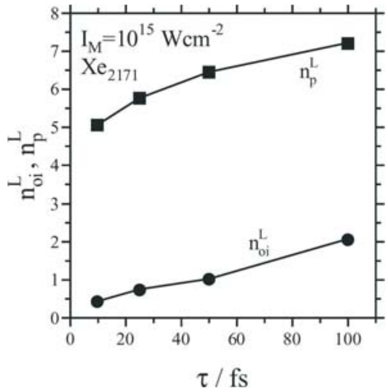

Fig. 4. The laser pulse length dependence of the long-time outer ionization levels of Xe_{2171} coupled to a laser field at $I_M = 10^{15}$ Wcm^{-2} ($\tau = 10$–100 fs). Ionization levels are presented for nanoplasma population (n_p^L, ■) and for outer ionization (n_{oi}^L, •).

with A being expressed in (Wcm^{-2})$^{-1/2}$ Å units. Equations (7) and (10) were utilized for the analysis of the long-time outer ionization levels n_{oi}^L (Sect. 2) in the intensity range and cluster size domain of the persistent nanoplasma existence. We assume that for a fixed value of the pulse length τ, ξ is weakly dependent on I_M and on R_0. From our MD simulations of CE driven by laser pulses with $\tau = 25$ fs, we find that ξ (Eq. (4a) at $t = 0$) for Xe_n ($n = 1061, 2171$) increases by <10% at $I_M = 10^{15}$ and 10^{16} Wcm^{-2}, while at $I_M = 10^{17}$ Wcm^{-2}, which constitutes a border case, ξ increases by 40–50%. The dependence of the long-time outer ionization level on the laser pulse length at fixed values of n and of I_M (Fig. 4) is attributed to the dependence of the expansion parameter ξ on τ. We expect that ξ will increase with increasing the pulse length, whereupon n_{oi} will increase with increasing τ.

The n_{oi}^L simulation results used for the exploration of the electrostatic model, equations (8) and (10), involved the following:

(i) for $\tau = 25$ fs, $n = 55$–2171 at $I_M = 10^{15}$–10^{16} Wcm^{-2} and $n = 1061$, 2171 at $I_M = 10^{17}$ Wcm^{-2};
(ii) for $\tau = 50$ fs, $n = 55$–2171 at $I_M = 10^{15}$ Wcm^{-2};
(iii) for $\tau = 100$ fs, $n = 55$–2171 at $I_M = 10^{15}$ Wcm^{-2} and $n = 2171$ at $I_M = 10^{16}$ Wcm^{-2};
(iv) for $\tau = 10$ fs scarce data for $n = 1061$ and 2171 at $I_M = 10^{15}$ Wcm^{-2} were used.

In Figure 5 we present the linear dependence of n_{oi}^L vs. $I_M^{1/2}/R_0$, according to equations (8) and (10), for the extensive data set (i) at $\tau = 25$ fs (Fig. 5a), which gives $\gamma^{1/2}\xi = 2.16$ and for the data set (iii) at $\tau = 100$ fs (Fig. 5b), which gives $\gamma^{1/2}\xi = 3.35$. The data set (ii) at $\tau = 50$ fs (not shown) also obeys well the linear n_{oi}^L vs. $I_M^{1/2}/R_0$ dependence resulting in $\gamma^{1/2}\xi = 2.42$, and the data set (iv) at $\tau = 100$ fs resulted in the estimate $\gamma^{1/2}\xi = 1.59$.

The central prediction of the CBSI model, which is confirmed by the simulation data, is the linear dependence of n_{oi}^L on $I_M^{1/2}/R_0$ (Figs. 5a and 5b). The foregoing analysis led to the cluster parameters $\gamma^{1/2}\xi$, which are determined by cluster expansions $\gamma^{1/2}\xi = 1.59$, 2.16, 2.42 and 3.35 at $\tau = 10$ fs, 25 fs, 50 fs and 100 fs, respectively. These parameters are independent of the initial cluster size (R_0) and laser intensity (I_M) in the region where the persistent nanoplasma prevails, which marks the validity domain of the electrostatic model, equations (8) and (10). Assuming that the correction parameter γ is weakly dependent on the pulse parameters and cluster size (an assumption justified by independent simulations of CE), this list of $\gamma^{1/2}\xi$ values provides the relative values of ξ at different pulse lengths. From the ion distribution data at the peak of the laser pulse ($t = 0$) presented in our previous work [11], we estimated the cluster expansion parameter $\xi = R(t = 0)/R_0 = 1.01$–$1.10$ at $\tau = 25$ fs ($I_M = 10^{15}$ Wcm^{-2} and 10^{16} Wcm^{-2}), so that at $t = 0$ the effects of CE set in for $\tau < 25$ fs, while for longer pulses ($\tau = 100$ fs) marked effects of CE are exhibited. The ratio of the cluster expansion parameters $\xi(\tau = 100\ \text{fs})/\xi(25\ \text{fs})$ at $I_M = 10^{15}$ Wcm^{-2} is 1.36 for Xe_{2171} and 1.42 for Xe_{1061}, as inferred from MD simulations of CE (at $t = 0$). This is in reasonable agreement with the ratio of 1.55 obtained herein from the τ dependence of the $\gamma^{1/2}\xi$ data for outer ionization.

The dependence of the compound parameter $\gamma^{1/2}\xi$ on τ can approximately be fit by the power law

$$\gamma^{1/2}\xi(\tau) = \xi_0\tau^{\alpha} \tag{11}$$

with $\alpha = 0.32 \pm 0.03$ and $\xi_0 = (0.75 \pm 0.03)^{-\alpha}$, while τ is given in fs. From equations (8), (10) and (11) we infer that the dependence of the outer ionization level on the cluster size and laser parameters (I_M and τ) can be recast in the form

$$n_{oi}^L = 1.06 \times 10^{-7}\tau^{0.64}I_M^{1/2}/R_0 \tag{12}$$

where R_0 is given in Å, I_M in Wcm^{-2} and τ in fs. It is gratifying that the relation between the outer ionization levels and the expansion parameter ξ, equation (4a), which incorporates the dependence of the pulse width according to equation (12), provides independent information on nuclear CE dynamics.

4 The border radius for outer ionization

The level of outer ionization of a cluster of radius R_0 can be specified by the cluster border radius [19,20,22] $R_0^{(I)}$ at the intensity I_M. Complete cluster outer ionization prevails for $R_0 < R_0^{(I)}$, while for $R_0 > R_0^{(I)}$ a persistent (positively charged) nanoplasma exists within the cluster after the termination of the laser pulse. $R_0^{(I)}$ constitutes the initial cluster radius prior to expansion driven by CE. We shall use the electrostatic model of Section 3 to provide an expression for $R_0^{(I)}$ for Xe_n clusters, which will be confronted with simulation results of electron dynamics.

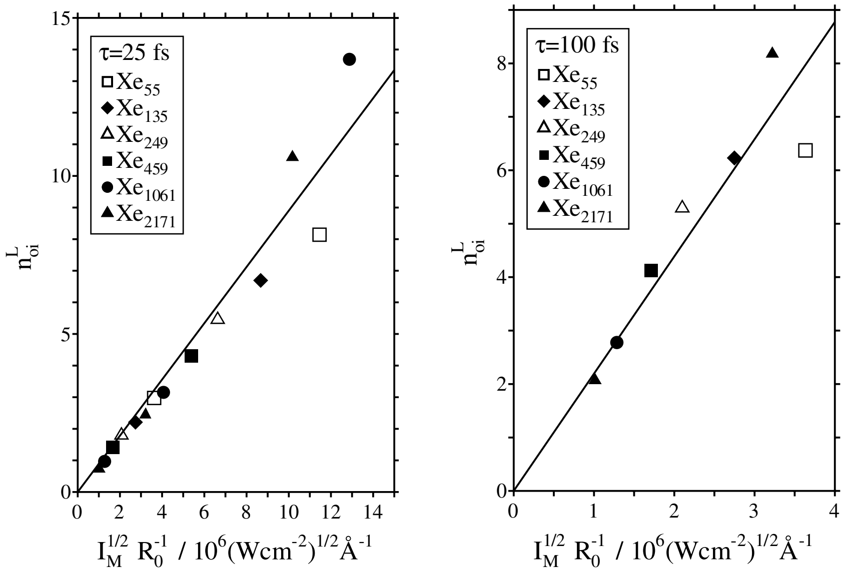

(a) (b)

Fig. 5. A test of the electrostatic model for outer ionization, which predicts a linear dependence of n_{oi}^L vs. $I_M^{1/2}/R_0$ over broad cluster size ranges and laser intensities at constant τ, when the persistent nanoplasma prevails in Xe_n clusters. (a) $\tau = 25$ fs, $n = 55$–2171 at $I_M = 10^{15}$–10^{16} Wcm^{-2} and $n = 1061$, 2171 at $I_M = 10^{17}$ Wcm^{-2}. (b) $\tau = 100$ fs, $n = 55$–2171 at $I_M = 10^{15}$ Wcm^{-2} and $n = 2171$ at $I_M = 10^{16}$ Wcm^{-2}.

The condition for complete outer ionization was obtained from the electrostatic model, equations (6) and (7). The characteristic maximal cluster radius $R_0^{(I)}$ for the attainment of the conditions $n_p^L = 0$ and $n_{oi}^L = n_{ii}^L = q_{av}$ (where q_{av} is the average charge of Xe^{q+}) is given by

$$R_0^{(I)} = F_M \gamma \xi^2 \bigg/ \left(\frac{4\pi\sqrt{2}}{3}\right) \bar{B} \rho_A q_{av}. \tag{13}$$

Utilizing equations (6), (10) and (13) results in

$$R_0^{(I)} = A I_M^{1/2} / q_{av} \tag{14}$$

which can be recast in the form

$$R_0^{(I)} = 1.9 \times 10^{-7} \gamma \xi^2 I_M^{1/2} / q_{av} \tag{15}$$

I_M is again given in Wcm^{-2}, R_0 in Å, and $R_0^{(I)}$ in Å. The average charge, q_{av}, in equation (14) incorporates the role of the intensity and cluster size dependence of the inner ionization level. We have used equations (14) and (15) for the estimates of $R_0^{(I)}$ in the intensity domain $I_M = 10^{15}$–10^{20} Wcm^{-2} and $\tau = 25$ fs, where $\gamma^{1/2}\xi = 2.16$ (Sect. 3). The values of the average charges q_{av} were taken from our previous work [11] for the appropriate values of I_M and for the cluster radius $R_0 = R_0^{(I)}$. The dependence of $R_0^{(I)}$ on I_M (at $\tau = 25$ fs) for Xe_n clusters is portrayed in Figure 6. Due to the marked increase of q_{av} with increasing I_M, the increase of $R_0^{(I)}$ with increasing $I_M^{1/2}$ is much weaker than the $R_0^{(I)} \propto I_M^{1/2}$ dependence, which is exhibited for $(\mathrm{D}_2)_n$ homonuclear clusters [19] and for $(\mathrm{CD}_4)_n$ clusters [20], reflecting some unique features of multiple ionization of heavy Xe_n clusters.

The results of the electrostatic model agree well with simulation results for outer ionization electron dynamics. The boundary radius $R_0^{(I)}$ can be inferred from the cluster size for complete outer ionization at a given laser intensity. $R_0^{(I)}$ for Xe_n clusters was obtained from simulation results for the attainment of the complete outer ionization level. In our simulations complete (taken as 95%) outer ionization was defined [19,20] by $n_{oi}(t = 0) = 0.95\, n_{ii}(t = 0)$ (taken at the peak of the Gaussian pulse at $t = 0$). The simulation results for $R_0^{(I)}$ at $I_M = 10^{16}$–10^{18} Wcm^{-2} ($\tau = 25$ fs) presented in Figure 6 are in satisfactory agreement (within 20%) with the predictions of the electrostatic model (Fig. 6). It is instructive to address the dependence of $R_0^{(I)}$ on the pulse length τ. Using equations (10)

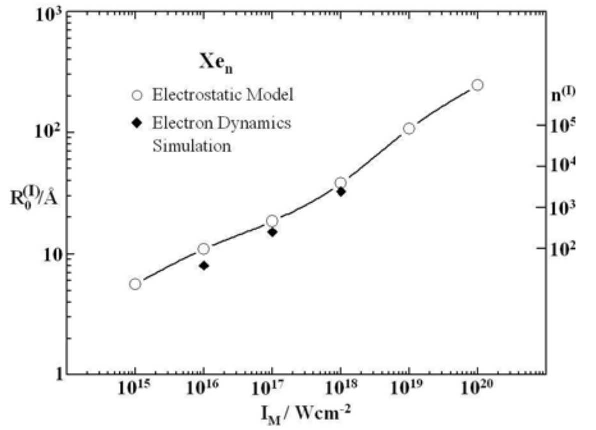

Fig. 6. The laser intensity dependence of the cluster border radius $R_0^{(I)}$ for complete cluster outer ionization and vertical ionization. The results of the electrostatic model (∘), equation (14), are in agreement with the simulation results for complete outer ionization (♦) (see text). The $n = n^{(I)}$ size of Xe_n clusters, corresponding to the border radius $R_0^{(I)}$, is also marked on the figure. Data of the electrostatic model are given for the intensity range $I_M = 10^{15}$–10^{20} Wcm^{-2} ($\tau = 25$ fs), while the simulation data are given for $I_M = 10^{16}$–10^{18} Wcm^{-2} ($\tau = 25$ fs).

and (11), together with equation (14), for the dependence of the expansion parameters ξ and τ, we obtain

$$R_0^{(I)} = 1.06 \times 10^{-7} \tau^{0.64} I_M^{1/2} / q_{av} \qquad (16)$$

for the boundary radius, where R_0 is given in Å, τ in fs, and I_M in Wcm^{-2}. The near linear dependence of $R_0^{(I)}$ on $\tau^{2\alpha}$ with $2\alpha = 0.64 \pm 0.06$ for Xe$_n$ clusters, according to equation (16), is identical with the value of $2\alpha = 0.62$ inferred for $(D_2)_n$ clusters [22]. The boundary radius, equation (16), marks the cluster size domain (specified in terms of the cluster initial radius R_0) for the existence of a persistent nanoplasma, which exists when $R_0 > R_0^{(I)}$. The boundary radius $R_0^{(I)}$, which emerges from the analysis of outer ionization electron dynamics, also specifies the upper limit of the cluster size for the applicability of the cluster vertical ionization (CVI) condition for nuclear CE dynamics [19,20,23], establishing the interrelationship between electron and nuclear dynamics in cluster-ultraintense laser interactions.

5 Discussion

We explored cluster-ultraintense laser interactions that drive electron dynamics of the nanoplasma in Xe$_n$ ($n =$ 55–2171) clusters. Of considerable interest is the production of a persistent nanoplasma in Xe$_n$ clusters at lower intensities of $I_M = 10^{15}$–10^{16} Wcm^{-2} and larger cluster sizes ($n =$ 459–2171), and a transient nanoplasma at higher laser intensities and smaller cluster sizes. It is instructive to attempt to establish contact between the microscopic nanoplasma model used herein and a macroscopic 'plasma model' for the nanoplasma response and outer ionization [8,9,14] that considers the enhancement of light absorption by resonance effects. The frequency of the linear oscillations for a thermally equilibrated and uniform nanoplasma is [7,8,14,15] $\omega_p = (4\pi e^2 \rho_e / 3m_e)^{1/2}$. The maximal (nearly intensity independent) electron density in the nanoplasma is $\rho_e^{max} = 0.08$–0.09 Å^{-3} (at $I_M =$ 10^{15}–10^{19} Wcm^{-2}, $\tau = 25$ fs), which is realized for the persistent nanoplasma ($I_M = 10^{15}$–10^{16} Wcm^{-2}) prior to cluster CE, and for the transient nanoplasma ($I_M >$ 10^{17} Wcm^{-2}) prior to its depletion. The nanoplasma energy is $\hbar\omega_p = 6.1$–6.4 eV. This value of $\hbar\omega_p$ is considerably larger than the photon energy of 1.44 eV. Our simulation results for the persistent nanoplasma at $I_M = 10^{15}$–10^{16} Wcm^{-2} over the time scale of $t - t_s = 100$ fs manifest the decrease of ρ_e due to CE. The time dependence of $n_{oi}(t)$ and $n_p(t)$ in this intensity domain (with $\tau =$ 25–100 fs) is smooth and does not reveal any steep temporal increase of the ionization level or the electron energy, which could be interpreted as resonance generation of nanoplasma oscillations, precluding the possibility of such excitations. The role of the macroscopic 'plasma model' [7,8,14,15] is not borne out by our simulations.

The gross features of the outer ionization process were adequately described by the electrostatic CBSI model [10], which predicts the linear dependence of n_{oi}^L vs. $I_M^{1/2}/R_0$, being in good agreement with simulation results, and being determined by the relative values of the cluster expansion parameter ξ and its pulse length dependence. In spite of this success of the electrostatic model, the complete description of outer ionization in terms of quasiresonance nonlinear effects in nanoplasma-laser interactions is still lacking. Some recent numerical simulations [10,24] and recently proposed macroscopic mechanisms involving surface absorption [25] pertain to this issue. Returning to the CBSI model, we have further pursued the electrostatic model for the estimates of the laser intensity and pulse width dependence of the cluster border radius $R_0^{(I)}$ for the completion of outer ionization, which is in reasonable agreement with simulation results for outer ionization and electron dynamics. The border radius $R_0^{(I)}$ is central in the characterization of the nuclear dynamics and energetics of CE [19,20,23]. In the cluster size domain and in the laser intensity range where $R_0 \leqslant R_0^{(I)}$, the cluster vertical ionization (CVI) model is applicable, with the energetics (e.g., the average ion energy E_{av}) of CE being characterized by the cluster size scaling equation $E_{av} \propto q_{av}^2 R_0^2$, which is explicitly independent of I_M and of other laser parameters [10,19,20,22,23]. The analysis of the energetics of CE of extremely charged ions from Xe$_n$ clusters [26] leads to independent estimates of $R_0^{(I)}$ at $I_M = 10^{16}$ Wcm^{-2} and at $I_M = 10^{17}$ Wcm^{-2}, which is in good agreement with the corresponding $R_0^{(I)}$ data from the electron dynamics (Fig. 6) presented herein. The border radius $R_0^{(I)}$ constitutes a bridge between electron (outer ionization) dynamics and nuclear (CE) dynamics in elemental and molecular clusters.

Another general characteristic of the dynamics of the nanoplasma, which is generated by near-infrared laser-cluster interaction, pertains to the strength of the charge hopping [27–31]. The electron-electron coupling Γ_{ee} and the electron-ion coupling Γ_{ei} are given by [30,31]

$$\Gamma_{ee} = e^2 / r_{ee}\epsilon \qquad (17)$$

and

$$\Gamma_{ei} = q_{av} \Gamma_{ee}^{3/2}. \qquad (18)$$

Here $r_{ee} = 2r_0/q_{av}^{1/3}$ is the interelectron separation, where $r_0 = 2.16$ Å is the Xe constituent radius, q_{av} is the average ionization level of each Xe atom [11], and ϵ is the nanoplasma single electron average energy [11]. The parameter Γ_{ei}, which represents the ratio of the ion charge to the electron charge within the Debye length, determines the length over which charge fluctuations are screened by nanoplasma electrons [29–31]. A weakly coupled nanoplasma is characterized by $\Gamma_{ee} \lesssim 0.1$ and $\Gamma_{ei} < 1$ [29–31]. In a weakly coupled electron-ion nanoplasma fluctuations resulting from the discrete nature of the charges, which give rise to collisions and Coulomb correlations, are kept at a low level through Debye shielding. For the persistent nanoplasma in Xe$_{2171}$ clusters driven by a near-infrared laser field, our simulations result in the following estimates of the coupling parameters in the intensity range and cluster size domain where the persistent nanoplasma prevails: for $I_M = 10^{15}$ Wcm^{-2} ($\epsilon = 53$ eV, $r_{ee} = 2.52$ Å, $q_{av} = 5$), $\Gamma_{ee} = 0.11$ and $\Gamma_{ei} = 0.18$. For $I_M = 10^{16}$ Wcm^{-2} ($\epsilon = 147$ eV, $r_{ee} = 2.16$ Å, $q_{av} = 8$), $\Gamma_{ee} = 0.045$ and $\Gamma_{ei} = 0.07$, while for $I_M = 10^{17}$ Wcm^{-2} ($\epsilon = 933$ eV, $r_{ee} = 1.75$ Å, $q_{av} = 15$) $\Gamma_{ee} = 8.8 \times 10^{-3}$ and $\Gamma_{ei} = 0.012$. The electron-electron and the electron-ion coupling parameters are lower than 0.2. Accordingly, the nanoplasma driven by near-infrared laser-elemental cluster interactions corresponds to the weak coupling limit, where ion-electron correlation and multi electron-ion collision effects are minor. The weakly coupled nanoplasma is realized at a low density limit, and at a high effective temperature. This situation is distinct from vacuum-ultraviolet-cluster interactions [32], where a strongly-coupled, electron-ion nanoplasma is produced, and many-body (multi electron-ion) collisions are important [31]. The main new results of this work pertain to the response of the nanoplasma in an elemental cluster driven by near-infrared laser fields. The computational results are amenable to description by electrostatic models for the effects of the cluster size, the laser intensity and the laser pulse length dependence of the nanoplasma depletion level and of the border radius for complete outer ionization.

This research was supported by the Deutsche Forschungsgemeinschaft (DFG) SFB 450 on "Analysis and Control of Ultrafast Photoinduced Reactions", and by the James-Franck Binational German-Israeli Program on Laser-Matter Interaction.

References

1. J. Jortner, Proc. Roy. Soc. Lond. A **356**, 477 (1998)
2. A.D. Bandrauk, N.H. Shon, Phys. Rev. A **66**, 031401 (2002); G.L. Kamta, A.D. Bandrauk, Phys. Rev. A **74**, 033415 (2006)
3. P.B. Corkum, Phys. Rev. Lett. **71**, 1994 (1993); V.R. Bhardwaj, P.B. Corkum, D.M. Rayner, Phys. Rev. Lett. **93**, 43001 (2004); C. Figueira de Morisson Faria, X. Liu, W. Becker, H. Schomerus, Phys. Rev. A **69**, 021402(R) (2004); E. Eremina, X. Liu, H. Rottke, W. Sandner, M. G. Schätzel, A. Dreischuh, G.G. Paulus, H. Walther, R. Moshammer, J. Ullrich, Phys. Rev. Lett. **92**, 173001 (2004)
4. M. Hentschel, R. Kienberger, Ch. Spielmann, G.A. Reider, N. Milosevic, T. Brabec, P. Corkum, U. Heinzmann, M. Drescher, F. Krausz, Nature **414**, 509 (2001); M. Kitzler, K. O'Keeffe, M. Lezius, J. Mod. Opt. **53**, 57 (2006)
5. M. Uiberacker, Th. Uphues, M. Schultze, A.J. Verhoef, V. Yakovlev, M.F. Kling, J. Rauschenberger, N.M. Kabachnik, H. Schröder, M. Lezius, K.L. Kompa, H.-G. Muller, M.J.J. Vrakking, S. Hendel, U. Kleineberg, U. Heinzmann, M. Drescher, F. Krausz, Nature **446**, 627 (2007)
6. T. Brabec, F. Krausz, Rev. Mod. Phys. **72**, 545 (2000); G.G. Paulus, F. Lindner, H. Walther, A. Baltuska, E. Goulielmakis, M. Lezius, F. Krausz, Phys. Rev. Lett. **91**, 253004 (2003); X. Liu, H. Rottke, E. Eremina, W. Sandner, E. Goulielmakis, K.O. Keeffe, M. Lezius, F. Krausz, F. Lindner, M.G. Schätzel, G.G. Paulus, H. Walther, Phys. Rev. Lett. **93**, 263001 (2004); C.C. Chirila, R.M. Potvliege, Phys. Rev. A **71**, 021402 (2005)
7. V.P. Krainov, M.B. Smirnov, Phys. Rep. **370**, 237 (2002)
8. U. Saalmann, Ch. Siedschlag, J.M. Rost, J. Phys. B **39**, R39 (2006)
9. I. Last, J. Jortner, Phys. Rev. A **62**, 013201 (2000)
10. I. Last, J. Jortner, J. Chem. Phys. **120**, 1336 (2004)
11. A. Heidenreich, I. Last, J. Jortner, Z. Phys. D **35**, 567 (2005); A. Heidenreich, I. Last, J. Jortner, J. Chem. Phys. **127**, 074305 (2007); A. Heidenreich, I. Last, J. Jortner, *Simulations of Extreme Ionization and Electron Dynamics in Ultraintense Laser-Cluster Interaction*, Isr. J. Chem. (special issue in honor of R.D. Levine), in press (2007)
12. M.D. Perry, G.A. Mourou, Sci. **264**, 917 (1994); J. Nees, N. Naumova, E. Power, V. Yanovsky, I. Sokolov, A. Maksimchuk, S.-W. Bahk, V. Chvykov, G. Kalintchenko, B. Hou, G. Mourou, J. Mod. Opt. **52**, 305 (2005); G.A. Mourou, T. Tajima, S.V. Bulanov, Rev. Mod. Phys. **78**, 309 (2006)
13. I. Last, J. Jortner, J. Chem. Phys. **120**, 1348 (2004)
14. T. Ditmire, Phys. Rev. A **57**, R4094 (1998); T. Ditmire, T. Donnely, A.M. Rubenchik, R.W. Falcone, M.D. Perry, Phys. Rev. A **53**, 3379 (1996); E. Springate, N. Hay, J.W.G. Tisch, M.B. Mason, T. Ditmire, M.H.R. Hutchinson, J.P. Marangos, Phys. Rev. A **61**, 063201 (2000)
15. F. Megi, M. Belkacem, M.A. Bouchene, E. Suraud, G. Zwicknagel, J. Phys. B **36**, 273 (2003)
16. F. Fennel, G.F. Bertsch, K.-H. Meiwes-Broer, Eur. Phys. J. D **29**, 367 (2004); T. Taguchi, T.M. Antonsen Jr, H.M. Milchberg, Phys. Rev. Lett. **92**, 205003 (2004)
17. T. Martchenko, Ch. Siedschlag, S. Zamith, H.G. Muller, M.J.J. Vrakking, Phys. Rev. A **72**, 053202 (2005)
18. G.M. Petrov, J. Davis, Phys. Plas. **13**, 033106 (2006)
19. I. Last, J. Jortner, J. Chem. Phys. **121**, 3030 (2004)
20. I. Last, J. Jortner, J. Chem. Phys. **121**, 8329 (2004)
21. U. Saalmann, J.M. Rost, Eur. Phys. J. D **36**, 159 (2005)
22. I. Last, J. Jortner, Phys. Rev. A **73**, 013202 (2006)
23. G. Chen, C. Wang, H. Lu, S. Li, J. Liu, G. Ni, R. Li, Z. Xu, J. Phys. B: At. Mol. Opt. Phys. **40**, 445 (2007)
24. Ch. Siedschlag, J.-M. Rost, Phys. Rev. A **67**, 13404 (2003); Ch. Siedschlag, J.-M. Rost, Phys. Rev. A **71**, 031401 (2005)
25. C. Jungreuthmayer, M. Geissler, J. Zanghellini, T. Brabec, Phys. Rev. Lett. **92**, 133401 (2004)
26. A. Heidenreich, I. Last, J. Jortner, *Energetics and Dynamics of CE of Xe_n Clusters* (in preparation)
27. A.N. Mostovich, L.Y. Chan, K.J. Kearney, D. Garren, C.A. Iglesias, M. Klapisch, F.J. Rogers, Phys. Rev. Lett. **75**, 1530 (1995)
28. M. Nantel, G. Ma, S. Gu, C.Y. Côté, J. Itatani, D. Umstadter, Phys. Rev. Lett. **80**, 4442 (1998)
29. G. Zwicknagel, C. Toepffer, P.-G. Reinhard, Hyp. Int. **99**, 285 (1996)
30. A. Müller, A. Wolf, Hyp. Int. **104**, 233 (1997)
31. C. Jugreuthmayer, L. Ramunno, J. Zanghellini, T. Brabec, J. Phys. B: At. Mol. Opt. Phys. **38**, 3029 (2005)
32. W. Wabnitz, L. Bittner, A.R.B. de Castro, R. Döhrman, P. Gürtler, T. Laarman, W. Laasch, J. Schulz, A. Swiderski, K. von Haeften, T. Möller, B. Faatz, A. Fateev, J. Feldhaus, C. Gerth, U. Hahn, E. Saldin, E. Schneidmiller, K. Sytchev, K. Tiedtke, R. Treusch, M. Yurkov, Nature **420**, 482 (2002)